Electrothermally balanced operation of solid oxide electrolysis cells

Skafte, Theis Løye; Rizvandi, Omid Babaie; Smitshuysen, Anne Lyck; Frandsen, Henrik Lund; Thorvald Høgh, Jens Valdemar; Hauch, Anne; Kær, Søren Knudsen; Araya, Samuel Simon; Graves, Christopher; Mogensen, Mogens Bjerg; Jensen, Søren Højgaard

Published in:
Journal of Power Sources

DOI (link to publication from Publisher):
10.1016/j.jpowsour.2022.231040

Publication date:
2022

Document Version
Publisher's PDF, also known as Version of record

Journal of Power Sources 523 (2022) 231040

Contents lists available at ScienceDirect

Journal of Power Sources

journal homepage: www.elsevier.com/locate/jpowsour

Electrothermally balanced operation of solid oxide electrolysis cells

Theis Løye Skafte [a,*,1], Omid Babaie Rizvandi [a], Anne Lyck Smitshuysen [a,2], Henrik Lund Frandsen [a], Jens Valdemar Thorvald Høgh [a], Anne Hauch [a], Søren Knudsen Kær [b], Samuel Simon Araya [b], Christopher Graves [a,c], Mogens Bjerg Mogensen [a], Søren Højgaard Jensen [b,c,d]

[a] Technical University of Denmark, Department of Energy Conversion and Storage, Anker Engelunds Vej 1, 2800, Kgs. Lyngby, Denmark
[b] Aalborg University, Department of Energy Technology, Pontoppidanstræde 111, 9220, Aalborg, Denmark
[c] Noon Energy Inc., Palo Alto, 94301, California, USA
[d] DynElectro ApS, 4621, Gadstrup, Denmark

HIGHLIGHTS

- A novel operation method for SOECs is developed for dynamic *power-to-X* systems.
- The method works by rapidly (ms) cycling between fuel cell and electrolysis mode.
- Stack temperature variation and associated thermomechanical stress is minimized.
- Lower degradation is observed, possibly due to higher impurities tolerance.
- Less nickel migration and agglomeration is observed relative to reference cells.

ARTICLE INFO

Keywords:
Electrolysis
Reversible
Thermoneutral
Power-to-X
Solid oxide cells
Dynamic operation

ABSTRACT

The ongoing green energy transition is increasing the need for dynamic and efficient *Power-to-X* (*PtX*) systems to convert surplus wind and solar power to high-value products. The solid oxide electrolysis cell (SOEC) technology offers the highest energy conversion efficiency. However, high degradation and thermal variations that cause thermomechanical stress hinders up-scaling of the SOEC technology. Here we present a novel operation method that alleviates temperature variations and minimize degradation caused by impurities and nickel migration. By rapidly switching between electrolysis mode and brief periods in fuel cell mode, a flat thermal profile is obtained. Our results thus establish a new, simple way to achieve increased SOEC stack and module size and extended lifetime. The new operation method enables dynamic operation of large SOEC modules for renewable energy powered *PtX* systems which could drastically decrease costs associated with production of high-value green fuels and chemicals from wind and solar power.

1. Introduction

Efficient energy conversion is required to enable the transition from fossil fuels to renewable energy [1]. The conversion of renewable electricity into gas or liquids is highly warranted, i.e. so-called *power-to-X (PtX)*. The most efficient technology for such conversions is the high-temperature solid oxide cell (SOC) [2,3], which can operate both as an electrolysis cell (SOEC, i.e. for *PtX*) and a fuel cell (SOFC) [4–6]. A reversible SOC can store electrical energy as stable gas or liquid, which can be converted back into electricity, and it can therefore act much like a battery. Unlike conventional batteries, SOC-based energy storage systems can store the energy in low-cost gas tanks or large underground caverns [7], rather than in expensive lithium-based batteries.

So far, limited long-term durability and high capital costs are the key challenges to large-scale implementation of the SOC technology [8]. Increasing the cell and stack size decreases the cost per unit output

* Corresponding author.
E-mail address: theis@noon.energy (T.L. Skafte).
[1] Present address: Noon Energy Inc., Palo Alto, 94301 California, USA.
[2] Present address: DynElectro ApS, 4621 Gadstrup, Denmark.

https://doi.org/10.1016/j.jpowsour.2022.231040
Received 22 November 2021; Received in revised form 10 January 2022; Accepted 17 January 2022
Available online 25 January 2022

(power, gas or liquid), but will also increase temperature variation in the SOEC stack. The temperature variation causes thermomechanical stresses in the stack, which increase variation in current density, the degradation rate, leak probability and ultimately cause device failure [9,10]. Upper thresholds for the temperature gradient across each cell suggested in literature range from 5 to 8 °C/cm [11,12]. Since the temperature is directly linked with cell resistance and overvoltage of the electrodes, and since overvoltage is linked to several degradation mechanisms [13,14], a large temperature variation across the stack can cause uneven cell degradation, which in turn reduces stack lifetime. Thus, the temperature variation in the stack, should ideally be less than 10 °C. However, up to 50–80 °C temperature variation inside the stack is often observed in state-of-the-art SOEC stacks and is largely tolerated by manufacturers [15].

High flow-rate gas circulation is one way to mitigate the high temperature gradients [11], but this approach complicates the balance-of-plant, lowers the efficiency and increases capital costs.

Electrolysis can be operated at the thermoneutral voltage (TNV; approximately 1.3 V for steam splitting and 1.5 V for CO_2 splitting), where the Joule heat production balances the reaction heat consumption [16]. This eliminates some of the challenges with thermal management [17], however, operation at TNV can lead to rapid degradation [18–20]. Furthermore, it would be desirable to operate at variable current densities to match variation in wind and solar power supply. This will, however, lead to temperature gradients in the stack. See Supplementary Note 1 for further discussion.

It was previously shown that reversible operation can essentially eliminate degradation at cell level for an 1100 h test [21]. Here, we will show that the same concept, but with lower cycle time, can be used and designed to mitigate temperature variations. If the cycle frequency is high enough, i.e. several times per second, no temperature changes are expected due to the thermal inertia of the large stack mass, as confirmed by Fu et al. [22] (Supplementary Note 2). So, we propose to substitute conventional galvanostatic or potentiostatic SOEC operation with a pulsed operation where an AC current (or voltage) is applied on top of a DC current (or voltage), an operating mode we refer to as AC:DC operation. By cycling asymmetrically around the open-circuit voltage (OCV) and operating most of the time in electrolysis mode, the technique can be applied to *PtX* for renewable production of fuels and chemicals instead of reversible operation like a rechargeable battery.

In the following, we first go through the experimental setups used to test this new method, and then thoroughly explain the theoretical concept and how it affects the temperature of the stack. Next, we show how it impacts the degradation rate by testing single cells in H_2O and CO_2 electrolysis, with and without gas cleaning. Lastly, we investigate the consequences at the microstructural level and provide a hypothesis for the observed lower degradation rate.

2. Experimental

2.1. Single-cell testing

The SOEC cells used for single-cell testing were all multi-layer tapecasted cells (MTC) cells produced at DTU Energy [20]. The cells have an active electrode area of 16 cm^2. On the air side, the cells have a 6–7 μm thick CGO barrier layer, a ~30 μm thick LSC-CGO oxygen electrode and LSC contact layer. On the fuel side, the cells have a ~300 μm thick Ni/3YSZ support layer and a 12–16 μm thick Ni/8YSZ fuel electrode. The Ni:YSZ volume ratio was 40:60 after reduction of NiO for all Ni/YSZ cermets. The electrolyte is made of 8YSZ. The MTC half-cells (Ni/3YSZ-Ni/8YSZ-8YSZ-$CGO_{barrier}$) were co-sintered at 1315 °C, cut into 53 × 53 mm^2 cells and the oxygen electrodes were applied and sintered at 930 °C. The tested cells are nominally the same but came from different production batches. For this reason, minor reproducibility issues could cause slight performance differences.

The setup used for testing SOEC cells has been presented previously [23], but some additional equipment was also used, as shown in Fig. S1. Asymmetric square shaped voltage waves were generated by a Weavetek function generator. The signal was amplified by a Kepco BOP 20-20D power supply operated in voltage mode. The Kepco current leads were connected to the SOEC cell. For CO_2 electrolysis, the average voltage was measured with a Branford 2286 digital multimeter and the average current was measured by the Kepco BOP 20-20D. For steam electrolysis, the average current and voltage was measured by a Keithley 2750 with a 7702 card. A Phillips oscilloscope was used to monitor the cell voltage and the signal from the function generator. The overall operating conditions for the H_2O electrolysis tests are presented in Supplementary Table 1. The cells were operated at 700 °C.

Three CO_2 electrolysis tests were conducted. A DC test with no gas cleaning, A DC test with gas cleaning and an AC:DC test starting with gas cleaning that was switched off after 260 h. The overall operating conditions for respectively the DC and AC:DC CO_2 electrolysis tests are presented in Supplementary Table 2. The inlet temperature was 695 °C.

Impedance measurements were obtained with a Solartron 1260 in a configuration presented elsewhere [24].

Data analysis was carried out and figures were created using the RAVDAV software package [25].

2.2. Stack testing

For stack testing, an SOFCMAN 302 stack with 30 NiO-YSZ|YSZ|GDC |LSCF-GDC (NiO: Nickel oxide, YSZ: Yttria-stabilized zirconia, GDC: Gadolinium-doped ceria, LSCF: $La_{0.6}Sr_{0.4}Co_{0.2}Fe_{0.8}O_{3-\delta}$) cells was used, each cell having a 63 cm^2 active electrode area [26,27]. The stack was sandwiched in a spring-loaded test fixture placed inside a furnace (Fig. S2). The spring loads are placed outside the furnace. Gas to the stack enters/exits the stack via the gas pipes connected to the test fixture. Current rods (behind the stack) provide current to the stack. The stack voltage was controlled with a bi-directional 1 kW Kepco BOP 50–20 power supply. The stack voltage was measured with a Tektronix TDS 3032 digital oscilloscope. During AC:DC testing, the measured electrolysis voltage was 36 V (1.2 V/cell) and the fuel cell voltage was 23 V (0.77 V/cell). The voltage frequency was 33 Hz, with 30 ms at 36 V and 3.3 ms at 23 V. The average voltage was 34.7 V (1.16 V/cell).

Data analysis was carried out and figures were created using the RAVDAV software package [25].

2.3. Microstructural investigation

Scanning electron microscopy (SEM) images were obtained using a Zeiss Merlin field emission scanning electron microscope. Samples were mounted in epoxy resin and polished. No conductive coating was applied to the sample surface, instead conductive tape was applied around the individual cells. The samples were electronically grounded to the sample stage in the microscope using conductive tape.

For image generation, an InLens SE detector was used and an accelerating voltage of 0.95 kV, a working distance of 4 mm and a probe current of 230 pA was applied. A scan rate of 20 s/frame was used to prolong the dwell time at the individual pixels to enhance the contrast in the images. This low-voltage in-lens SEM imaging technique is described in detail by Thydén et al. [28].

2.4. COMSOL modeling

A multiscale model including transport equations of mass, momentum, species, charges, and heat was used in this study. This approach was taken to solve the many coupled equations in multiple dimensions over thousands of cycles to reach equilibrium in the cycling. To obtain the multiscale model the interior layered domains of the stack were represented through homogenization to obtain effective representative modeling variables for an equivalent porous domain. The application of this approach to the active area of the stack was

introduced by Navasa et al. [29], and the addition of the headers, sealing, and manifolds to the model have been recently done by Miao et al. [30] and further elaborated in Rizvandi et al. [31]. The 3D geometry of the stack is shown in Fig. S3.

Using the 3D model for the AC:DC operation mode was not computationally feasible as it resolved each cycle in about 1 h depending on the operating conditions. Therefore, an hour simulation of the AC:DC mode with the 3D model would take about 13.5 years of runtime. However, an equivalent 1D model, shown in Fig. S3, based on the same homogenization approach resolved each cycle in less than 10 s and so an hour simulation of the AC:DC operation mode could be completed within two weeks. The 1D model describes the variation of parameters along the flow direction and included all the domains except the manifolds. It was verified against the 3D model showing good consistency. The 1D simplification entails that the same voltage drop was applied to all the cells, and heat transfer between the cells was not considered.

Inlets and outlets were located at the left and right edges of the modeling domain, respectively, which resulted in a co-flow configuration. Atmospheric pressure was set to the outlets, and inlet pressure was applied to the fuel side. Moreover, the operation temperature was applied to the model through the gas inlet temperatures. The new cycling operation mode was applied to the model via rectangular pulses of the cell voltage, cycling between electrolysis and fuel cell voltages, as shown in Fig. S4 for the first 500 ms of the operation.

It should be noted that OCV is set to the first cycle, and the cycling operation started from the second cycle. Smoothing with a size of transition of 25% of the constant voltage time step is used to minimize the convergence difficulties and improve the runtime of the model. The initial evolution of the average current density over the active area corresponding to the operation voltage are also shown in Fig. S4. The operating conditions are listed in Supplementary Table 2 and were selected to simulate partial conversion of the steam in three serially connected stacks, i.e. to simulate the first stack in a large SOEC module (a module consists of many stacks in one thermal enclosure). The gas inlet and outlet temperature were 700 °C and 710 °C, respectively.

The inlet and outlet gas composition were pH_2O:pH_2 0.90:0.10 and pH_2O:pH_2 0.70:0.30, respectively. The DC operation was fixed at 1.25 V, while the AC:DC operation was 90% of the time at V_1, 1.25 V, and 10% at V_2, 0.704 V, with a cycle frequency of 30 Hz. The current densities were -0.39 A/cm^2 and -0.41 A/cm^2 for constant and cycling operation, respectively. Detailed discussion of the modeling approach and geometric and modeling parameters can be found in Refs. [29,30].

COMSOL Multiphysics software was used to couple the governing equations and solve them numerically via the finite element method approach. A mesh size of 1 mm was applied to all domains with 5 times improved mesh density at the inlet and outlet of the active area, which led to a number of degrees of freedom of 1694. The model was run on a high-end workstation with an Intel Core i9 3.5 GHz 12-core processor.

3. Results and discussion

3.1. Theoretical framework

By adding rapid reverse pulses to the direct current (or voltage), we show that it is possible to decouple the hydrogen production rate and the temperature inside the SOEC. The approach is illustrated in Fig. 1. By controlling the shape and frequency of the pulses, the new operation method enables dynamic operation, even with large stacks and modules, without generating temperature gradients and associated disadvantages.

By rapidly switching between electrolysis (endothermic operating point below TNV) and fuel cell mode (exothermic), the combined stack temperature can be controlled accurately by choosing the electrolysis voltage (V_1), the fuel cell voltage (V_2), the time spent at V_1 and V_2 for each cycle (t_1 and t_2), and the frequency of switching (f). To avoid any issues related to power electronics when scaling to MW systems, more

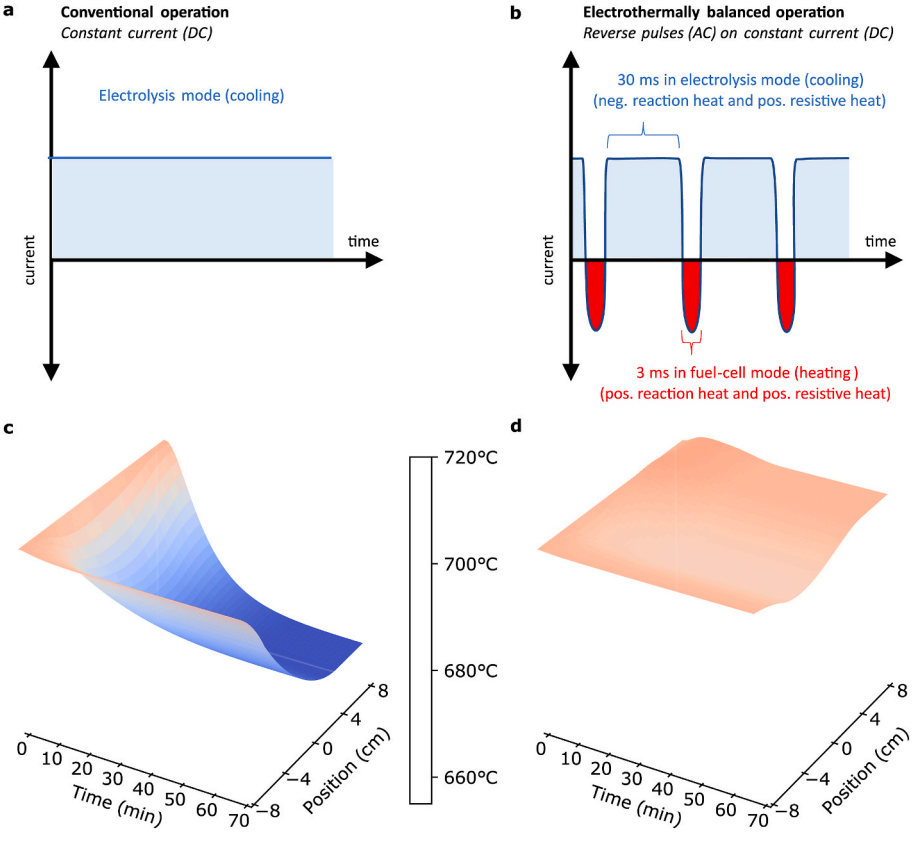

Fig. 1. Illustration of conventional operation (DC) and the new electrothermally balanced (AC:DC) operation. (a) conventional operation below thermoneutral voltage, (b) electrothermally balanced operation where the exothermal heat generation during short reverse pulses in fuel cell mode plus Joule heat in both electrolysis and fuel cell mode counterbalance the reaction heat required in electrolysis mode. The cycle duration is kept sufficiently short (in this example 3 ms + 30 ms) to avoid temperature variation during each cycle. (c)–(d), COMSOL modelled temperature profiles across a stack operating in DC mode, (c), and AC:DC mode, (d).

elaborate voltage curves can be incorporated with a gradual transition with a duration of a few milliseconds (ms) from one voltage level to the other. For the system to operate thermoneutrally during cycling, each cycle is designed to have one heat consuming and three heat producing contributions, as described by equation (1).

$$t_1 \cdot \left(Q_{r,1} + Q_{J,1}\right) + t_2 \cdot \left(Q_{r,2} + Q_{J,2}\right) = 0 \quad (1)$$

The endothermic reaction heat, $Q_{r,1}$, during operation at V_1 (SOEC mode) is negative; the exothermic reaction heat, $Q_{r,2}$, during operation at V_2 (SOFC mode) is positive; and the exothermic Joule heat, $Q_{J,1}$ and $Q_{J,2}$, at V_1 and V_2, respectively, are both positive. It is important to realize that net electrolysis operation can be achieved, since the two Joule heat contributions are both positive. Thus, the temperature can be controlled electronically at the local reaction sites, and the temperature variation through the stack can thus be minimized. In other words, AC:DC electrolysis operation is a way of supplying the necessary heat locally to where it is needed, rather than through an up-stream external electrical heat source.

Conventional stack operation below TNV leads to a temperature drop inside the stack. As exemplified with a COMSOL model of a 30-cell stack in Fig. 1c–d, this leads to an uneven current density distribution (Fig. S5), due to the increased resistance in the part of the stack where the temperature is low (Fig. 1c). The model details are presented elsewhere [31,32]. We note that it is possible to operate with a minimal temperature gradient if the voltage is fixed at the TNV. Operating the stack with the AC:DC technique eliminates the steep temperature drop (Fig. 1d) and thus also flattens the current density profile (see Fig. S5b). A small temperature variation from gas inlet to outlet is still seen for AC:DC operation due to the gradual increase in Nernst voltage from inlet to outlet.

Besides the mentioned challenges for conventional operation, temperature variation inside SOEC stacks becomes even more critical for operation with CO_2 (e.g. for *PtX* production of hydro-carbon based fuels) where a larger temperature difference across the cell (and stack) can easily push the operating point outside the desired operating window and cause localized carbon formation, which fractures the cell [13,33,34].

In the following we complement the theoretical modeling with experimental results showing that AC:DC operation 1) decouples stack temperature and hydrogen production rate, and 2) reduces degradation rate, on account of a lower overvoltage, reduced Ni-migration and an impurity expelling effect, exemplified with a steam electrolysis test and a CO_2 electrolysis test with as-supplied (not cleaned) and cleaned CO_2/CO gas.

3.2. Effect on stack temperature

An SOFCMAN 302 stack with 30 cells is operated first with conventional DC operation and then with the new AC:DC method. The operating temperature is approximately 694 °C with 76% H_2O + 24% H_2 as feed gas and air to the oxygen electrode. In DC mode, the stack is switched from OCV to an applied voltage of 34.4 V (potentiostatically), corresponding to 1.150 V for each cell. The measured average current density is −0.15 A/cm^2. With a measured OCV of 0.919 V (average per cell), and a TNV of 1.283 V, the stack is operated endothermically. This is confirmed with a thermocouple placed on the stack surface, which shows that the stack surface temperature is dropping ~1.7 °C when the voltage is applied (Fig. 2).

In AC:DC mode the voltage is switched between V_1 = 36 V and V_2 = 23 V (90% of the time at V_1) with a frequency of 33 Hz (Fig. S6), yielding an average voltage of 34.7 V for the stack or 1.16 V per cell. The average current density during AC:DC operation is −0.15 A/cm^2, and thus comparable to the above experiment. For additional data, see Fig. S7. For AC:DC operation a temperature increase of ~2 °C is achieved (Fig. 2). This illustrates how it is possible to change the temperature of the stack without changing the electrolysis output (hydrogen production rate). With other AC:DC parameters, it is also possible to keep the temperature profile entirely flat. Thus, in agreement with the modeling results, the stack testing confirms that the AC:DC operation method makes it possible to tailor the temperature profile while keeping a fixed current density (and gas production rate).

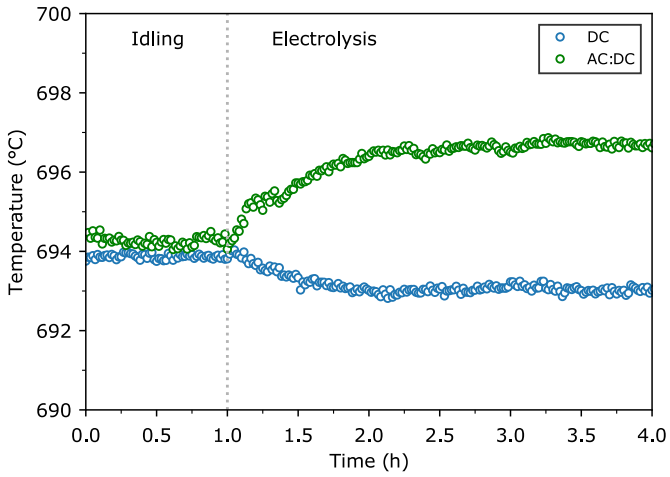

Fig. 2. Stack temperature while testing a 30-cell SOFCMAN 302 stack in DC and AC:DC mode. In DC mode, a temperature drop is observed in contrast to AC:DC operation where a temperature increase is achieved. The stack is operated at 694 °C with pH_2O:pH_2 0.76:0.24 and air to the negative and positive electrodes, respectively (H_2 120 L/h, H_2O 384 L/h and air 1200 L/h). The temperature is measured on the external top-plate of the stack.

3.3. Decreasing degradation

State-of-the-art fuel electrode supported SOECs with 16 cm^2 active electrode area (see section 2.1 and Hauch et al. [20] for further details) are tested to investigate the effect of the new operating mode on the degradation rate. First, two nominally identical cells are tested as H_2O electrolyzers with and without the AC:DC operating mode. The cells are operated at 700 °C with an inlet gas composition of 50% H_2O in H_2 for a few hundred hours. Operating voltage and current are reasonably standard for a conventional DC cell test, i.e. 1.270 V and −0.73 A/cm^2. For the AC:DC cell test, the voltage is set to fluctuate with a frequency of 30 Hz between V_1 = 1.270 V and V_2 = 0.800 V with 90% of the time at V_1, which yields −0.55 A/cm^2 on average. To isolate the effect of the operating modes, the inlet gas is cleaned by passing it through crushed Ni and yttria-stabilized zirconia powder at a temperature 25 °C below the cell operating temperature. H_2S (and other) impurities present in the gas will preferentially adsorb on the Ni particles in the gas cleaning unit before entering the cell. This has previously been shown to have a pronounced effect on the degradation rate [23,33].

As seen in Fig. 3a, the degradation rate for the AC:DC cell test is noticeably lower than for the DC test. In fact, with a rate of −6 mΩ cm^2/kh, the cell is seen to activate slightly during the full 450 h of operation. After the initial activation in the first ~150 h, though, the degradation is seen to stabilize at 15 mΩ cm^2/kh. The cell tested in DC mode degrades steadily with 108 mΩ cm^2/kh after the initial ~50 h activation. A degradation rate of 108 mΩ cm^2/kh is only slightly higher than recent state-of-the-art electrolysis tests reported in literature [35–38], and can thus be considered representative of a state-of-the-art cell. Despite the lower average current density for the AC:DC cell test, the total H_2 production will far outweigh the DC test due to the much longer expected lifetime.

Further investigation of the electrochemical impedance confirms the slight activation for the AC:DC operated cell. Electrochemical impedance spectroscopy (EIS) shows that the total resistance of the cell

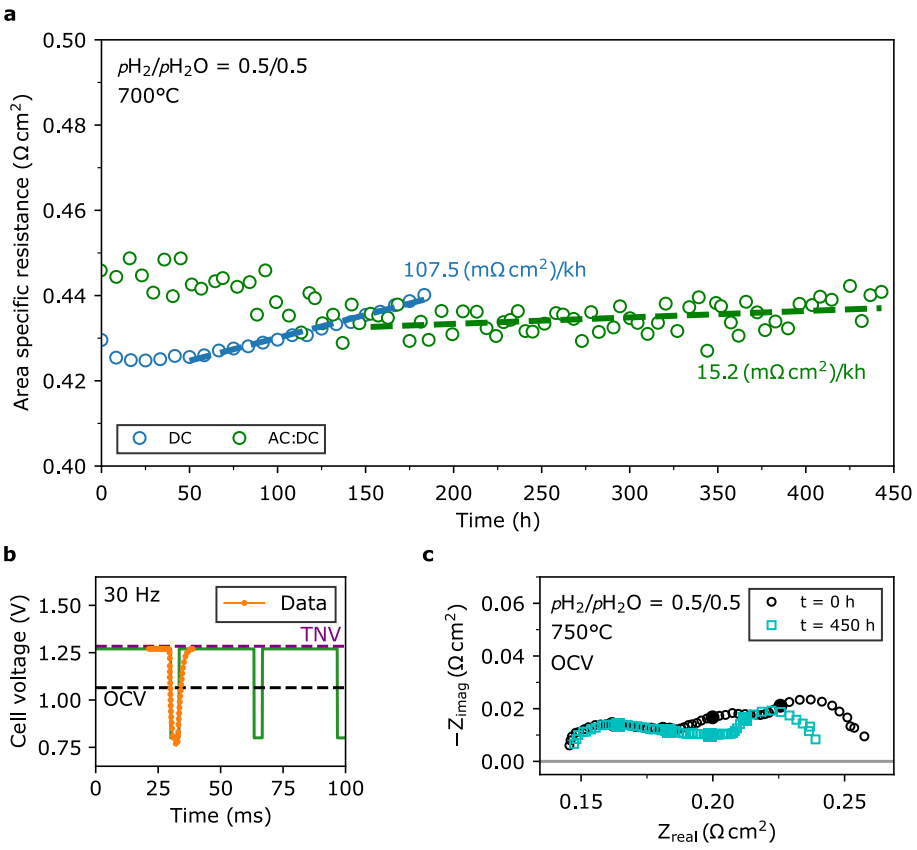

Fig. 3. Conventional H_2O electrolysis compared to electrothermally balanced AC:DC electrolysis with 16 cm^2 SOEC cells operated at 700 °C with an inlet gas of 50% H_2O in H_2. Inlet fuel gas is cleaned for both tests. (a) Resistance of each cell during the first few hundreds of hours of operation. Linear fits are shown as dashed lines, with the first 50 h and 150 h excluded for the DC and AC:DC test, respectively. Only every 20th data point at electrolysis voltage, i.e. V_1, are shown for the AC:DC test. (b) The voltage profile used for the AC:DC operation. Orange markers show an example of the actual data measured with an oscilloscope. The green line shows the voltage setpoint. (c) Nyquist plot of impedance data of the AC:DC cell before and after 450 h of operation, recorded at 750 °C and at OCV with 50% H_2O in H_2. (For interpretation of the references to colour in this figure legend, the reader is referred to the Web version of this article.)

decreases by 20 mΩ cm^2 from 260 to 240 mΩ cm^2 at 750 °C, when measuring at OCV before and after testing (Fig. 3c). The main difference is found at around 90 Hz, as seen in Fig. S8.

3.4. Impurity expelling ability

Next, to test the tolerance of the AC:DC operating mode towards gas

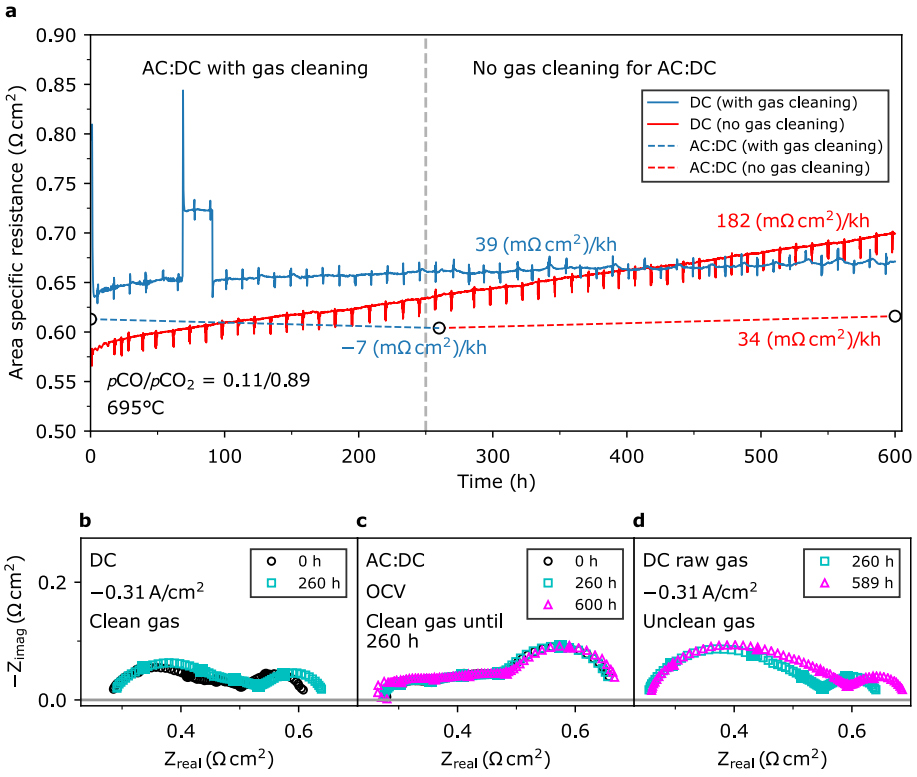

Fig. 4. The effect of electrothermal operation on CO_2 electrolysis with impure gas feed. Three 16 cm^2 SOEC cells are operated at 695 °C with an inlet gas of ~90% CO_2 in CO. Inlet fuel gas is cleaned for the gas cleaned DC test and the first 250 h of the AC:DC test. After the initial 250 h, the gas cleaning unit is turned off for the AC:DC test. (a) Area specific resistance for the three cells during the first 600 h of testing. Resistance is calculated using Ohm's law for the DC tests and from a Branford multimeter for the first measurement during the AC:DC test. EIS measurements at OCV for the AC:DC test are used to estimate the degradation rate during testing. (b) EIS of the DC test with gas cleaning during operation for the first 260 h with −0.31 A/cm^2. (c) EIS of the AC:DC test at OCV initially, after operation with a gas cleaner (first 260 h) and after operation without a gas cleaner (last 340 h). (d) EIS for the DC test without gas cleaning during operation with −0.31 A/cm^2 for the same time period as the AC:DC test without gas cleaning. Operating current is −0.31 A/cm^2 and −0.30 A/cm^2 (average) for DC and AC:DC operation, respectively. For AC:DC operation, a frequency of 30 Hz is applied between V_1 = 1.300 V and V_2 = 0.750 V with 60% time at V_1. Total gas flow to the negative electrode is 10.5–18 L/h and air flow to the positive electrode is 50 L/h and 140 L/h for DC and AC:DC operation, respectively.

impurities, three nominally identical cells are tested as CO_2 electrolyzers. The two cells tested in DC mode are reported in Hauch et al. [14]. Impurities play a substantial role when electrolyzing CO_2 with SOECs, where as little as a few ppb H_2S can detrimentally affect lifetime of the cell [23,33]. The sulfur will adsorb on the electrocatalyst, typically Ni, and block the reaction site. Thus, CO_2/CO is a suitable atmospheric environment to benchmark the general sulfur tolerance of AC:DC operation.

As shown in Fig. 4, cleaning the inlet gas is crucial for obtaining a reasonably low degradation rate. Conventional operation of state-of-the-art cells at 695 °C with an inlet gas composition of 89% CO_2 in CO, straight from the gas bottles, yields a degradation rate of 182 mΩ cm^2/kh. Such high degradation rate is not uncommon for CO_2 electrolysis when operating without a gas cleaning unit [23,33]. Under these conditions and assuming continued linear degradation, the time it takes to double the resistance is < 1 year and the cell will also reach TNV after <1 year, if operated galvanostatically. These time periods will be referred to as extrapolated lifetimes in this paper.

Cleaning the inlet gas lowers the degradation rate dramatically. The gas is cleaned in the same manner as previously described [23,33]. For a nominally identical cell, the rate is now 39 mΩ cm^2/kh, yielding extrapolated lifetimes of 1.2 years before doubling of the resistance or 3.4 years before reaching TNV.

If operating a cell in AC:DC mode, however, the degradation rate remarkably decreases when cleaning the inlet gas during the first 250 h, and then when the inlet gas is not cleaned it still exhibits a low degradation rate of 34 mΩ cm^2/kh for the last 340 h of the test (Fig. 4a), as measured with EIS at OCV before and after the test (Fig. 4c). Resistance measured with a Branford multimeter during operation confirms the degradation rate. The degradation rate of 34 mΩ cm^2/kh, when the inlet gas is not cleaned, gives an extrapolated lifetime of 2.2 years before doubling of the resistance. E_{Nernst} is 0.877 V and with a current density of −0.3 A/cm^2, a doubling of the initial AC:DC resistance will yield a final average cell voltage around 1.12 V, i.e. well below the TNV (1.47 V) for CO_2 electrolysis. See Table 1 for an overview of the degradation rates and the extrapolated lifetimes. Measuring EIS in H_2/H_2O before and after AC:DC testing confirms that the cell has not degraded (Fig. S9). See Fig. S10 for the AC:DC profile.

The exact mechanistic explanation for the observed lower degradation rate is not fully understood, but the authors speculate that it may be caused by electrochemical oxidation/reduction of adsorbed impurities followed by desorption due to a higher vapor pressure for the oxidized/reduced species. Alternatively, the impurity desorption can occur via a chemical reaction coupled to the local change in the partial pressure of reactants/products at the triple-phase boundary (TPB), i.e. via Le Chatelier's principle. One example of such an impurity adsorption/desorption mechanism is the formation/removal of SiO_2 at the active sites during cathodic/anodic polarization of the Ni/YSZ electrode [39]. During cathodic polarization, the local steam partial pressure is low at the TPB. The low steam partial pressure results in a shift in the equilibrium concentration for $Si(OH)_4$ and SiO_2, which results in SiO_2 formation at the TPB via reaction (2):

$$Si(OH)_4\ (g) = H_2O\ (g) + SiO_2\ (l) \quad (2)$$

Table 1
Degradation rates and extrapolated lifetime of CO_2 electrolysis tests.

Electrolysis mode	Gas Cleaning	Degradation rate (mΩ cm^2/kh)	Extrapolated lifetime before doubling resistance (years)	Extrapolated lifetime before TNV (years)
DC	No	182	<1	<1
DC	Yes	39	1.2	3.4
AC:DC	No	34	2.2	4.4
AC:DC	Yes	−7	∞	∞

During a short anodic polarization, H_2O may be formed and SiO_2 may be desorbed via formation of vapor-phase $Si(OH)_4$, which then leaves the electrode together with the produced H_2. In a similar manner, it is expected that the anodic pulses applied during AC:DC mode can desorb adsorbed sulfur species and other impurities, similar to what has been demonstrated for CO during dynamic testing of proton-exchange membrane fuel cells [40,41].

Likewise, for CO_2 electrolysis, we expect adsorption and re-oxidation of adsorbed monoatomic carbon on the Ni particle surfaces can be coupled to the electrode polarization via Le Chatelier's principle and take place via the Boudouard reaction:

$$2CO\ (g) = CO_2\ (g) + C\ (s) \quad (3)$$

With a carbon surface concentration in the ppm range, this reaction mechanism can explain the extraordinarily high capacity observed for the gas conversion impedance measured during CO_2 electrolysis [42].

AC:DC operation increases the gas outlet temperature (as shown in Fig. 1c–d). For CO_2 electrolysis, the higher outlet temperature enables an increase in the CO outlet gas concentration due to the shift in the Boudouard equilibrium towards a decreased carbon activity. Coupled with carbon re-gasification this can improve commercial SOEC-based on-site CO production such as Haldor Topsoe's eCOs™ technology [43].

3.5. Reduced Ni migration

Another intriguing theory for the lower degradation rate observed for AC:DC operation is that the AC:DC operation alters the wetting of the Ni particles in the fuel electrode or the oxide ion defect concentration at the Ni/YSZ interface [38]. Ni migration is a major contributor to degradation of current SOECs [44,45]. Based on SEM images using a low-voltage technique [46] (Fig. 5), AC:DC operation led to a dramatic reduction in Ni migration near the fuel electrode/electrolyte interface as well as suppressed Ni agglomeration in the support layer. Cells that either ran with conventional DC operation without gas cleaning (Figs. 5a and 780 h) or for an extended time period (Figs. 5b and 5000+ h) – the red and blue data shown in Fig. 5a, respectively – both showed significant Ni migration. The cell running with AC:DC shows no signs of Ni migration (Fig. 5c) and is indistinguishable from a reference cell that had only been heated up and reduced (Fig. 5d). For further information on the two DC cell tests, the reader is referred to the detailed investigation of those tests as reported in Hauch et al. [14]. It is entirely possible that the higher tolerance of impurities and the reduced Ni migration are linked. As discussed in Mogensen et al. [45], a lower susceptibility to blockage by impurities could lead to less Ni migration, perhaps due to a lower overpotential on the Ni particles.

4. Conclusions

The high efficiency along with the ability of the SOC to operate as both a fuel cell and an electrolyzer makes it ideal for long-term and large-scale energy storage or for production of gas or liquid from intermittently available renewable power. Here we have shown how thermal gradients in endothermal operating conditions can be mitigated by operating the stack in a novel manner. By overlaying an AC voltage on top of the DC voltage, the temperature profile is kept flat across the cell. This significantly reduces thermal stress caused by temperature gradients and local hotspots of high overpotential or high production rate, all of which can lead to severe degradation and failure. With stack testing and multiphysics modeling we show that the new operating mode does indeed flatten the temperature profile across the stack. In addition to the flat temperature profile, the AC:DC operating method provides additional advantages for substantially enhancing the lifetime. AC:DC operation show improved tolerance towards impurities as it may prevent the nucleation of an impurity phase (e.g. SiO_2) or unwanted phase (carbon) at the 3PB. Lastly, preliminary results on the effect of the

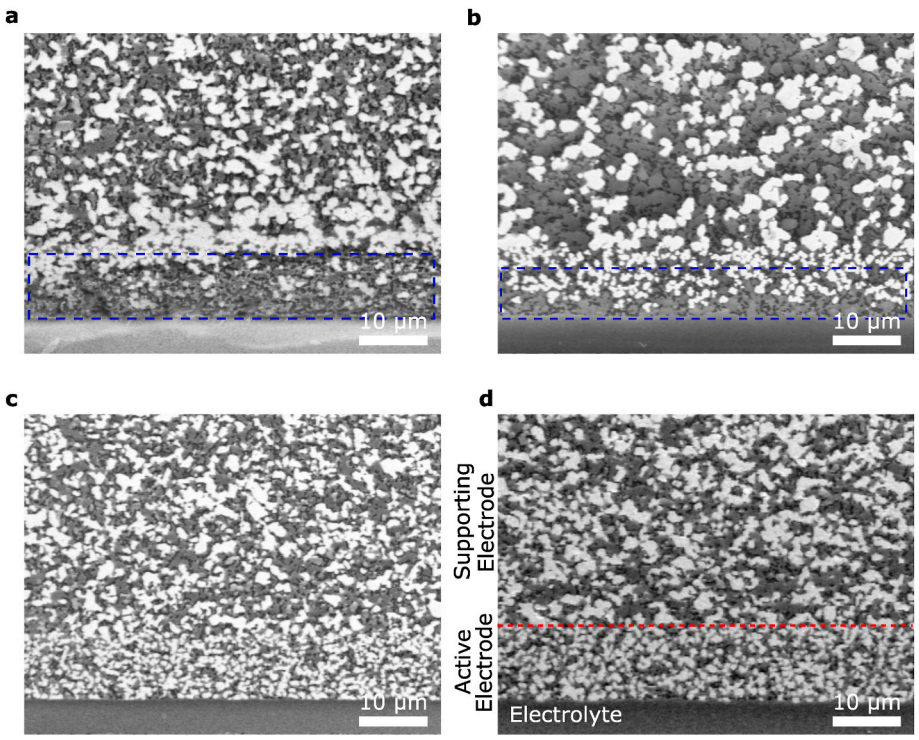

Fig. 5. Reduced Ni migration when operating with AC:DC. Scanning electron microscopy in low voltage mode to highlight interconnected Ni (bright white particles) in the active electrode near the electrolyte and the supporting electrode layer. (a) Cell operated in DC mode with −0.31 A/cm^2 for 780 h at 695 °C with an inlet gas of ~90% CO_2 in CO without a gas cleaning unit. The operating voltage increased exponentially and eventually reached more than 1.8 V as reported in Hauch et al. [14]. Significant Ni migration and agglomeration is observed. The depleted Ni zone is indicated by the blue dashed rectangle. (b) Cell operated in DC mode with −0.31 A/cm^2 for more than 5000 h at 695 °C with an inlet gas of ~90% CO_2 in CO with a gas cleaning unit [14]. Degradation was steady and cell voltage stayed below 1.4 V. Some Ni migration and significant Ni agglomeration in the supporting layer is observed. The depleted Ni zone is indicated by the blue dashed rectangle. (c) Cell operated in AC:DC mode with an average current density of −0.30 A/cm^2 for 600 h at 695 °C with an inlet gas of ~90% CO_2 in CO with a gas cleaning unit for the first 260 h and without one for the last 340 h. No Ni migration or agglomeration is observed. (d) Reference cell that was only heated up, reduced and then cooled again. No Ni migration or agglomeration is observed. (For interpretation of the references to colour in this figure legend, the reader is referred to the Web version of this article.)

operating mode on the electrode microstructure are highly promising, as no Ni migration or agglomeration is observed, which may be related to the lower degradation rate and electrode overpotential, and thus linked to the tolerance towards impurities.

In the future, further optimization of the parameters of the operating method will be carried out, but the basic framework has been outlined in this paper. Longer testing of cells with and without impurities in the inlet gas stream may further elucidate the beneficial effects on degradation mechanisms, e.g. Ni migration and poisoning with impurities. Testing of large stacks with thermocouples inserted throughout the stack volume may clarify the limitations of the electrothermally balanced operation in terms of stack size.

We expect that the method will be tested on other electrolysis technologies to investigate any potential issues or additional benefits. We further anticipate that this novel operating method will have great impact on both the scale-up and lifetime of the SOC, which are key to achieving cost-effective production of green fuels and chemicals from solar and wind power in the form of chemicals.

Funding

We gratefully acknowledge financial support from Independent Research Fund Denmark (case 9035-00014B), DTU Risø Reaktor (case RFS-17-0012), Innovation Network Smart Energy (case "Dynamisk Elektrolyse"), and Innovation Fund Denmark (case 8062-01638B).

CRediT authorship contribution statement

Theis Løye Skafte: Data curation, Formal analysis, Investigation, Methodology, Project administration, Resources, Visualization, Writing – original draft. **Omid Babaie Rizvandi:** Data curation, Investigation, Methodology, Software, Writing – review & editing. **Anne Lyck Smitshuysen:** Data curation, Investigation, Writing – review & editing. **Henrik Lund Frandsen:** Project administration, Resources, Software, Writing – review & editing. **Jens Valdemar Thorvald Høgh:** Investigation, Resources. **Anne Hauch:** Investigation, Resources, Writing – review & editing. **Søren Knudsen Kær:** Conceptualization. **Samuel Simon Araya:** Conceptualization, Writing – review & editing. **Christopher Graves:** Conceptualization. **Mogens Bjerg Mogensen:** Conceptualization, Writing – review & editing. **Søren Højgaard Jensen:** Conceptualization, Data curation, Formal analysis, Funding acquisition, Investigation, Methodology, Project administration, Resources, Visualization, Writing – original draft.

Declaration of competing interest

The authors declare that they have no known competing financial interests or personal relationships that could have appeared to influence the work reported in this paper.Authors declare competing interests regarding DynElectro ApS, which is commercializing the methods described in this paper and of which A.L.S. is an employee and S.H.J. is the CEO. S.H.J. and DynElectro ApS holds a patent for the described method.

Acknowledgments

We thank Samantha Jane Phillips for producing Fig. 1a–b.

Appendix A. Supplementary data

Supplementary data to this article can be found online at https://doi.org/10.1016/j.jpowsour.2022.231040.

References

[1] S.J. Davis, N.S. Lewis, M. Shaner, S. Aggarwal, D. Arent, I.L. Azevedo, S.M. Benson, T. Bradley, J. Brouwer, Y.-M. Chiang, C.T.M. Clack, A. Cohen, S. Doig, J. Edmonds, P. Fennell, C.B. Field, B. Hannegan, B.-M. Hodge, M.I. Hoffert, E. Ingersoll, P. Jaramillo, K.S. Lackner, K.J. Mach, M. Mastrandrea, J. Ogden, P.F. Peterson, D. L. Sanchez, D. Sperling, J. Stagner, J.E. Trancik, C.-J. Yang, K. Caldeira, Net-zero emissions energy systems, Science 360 (2018), eaas9793, https://doi.org/10.1126/science.aas9793.

[2] D. Ferrero, A. Lanzini, M. Santarelli, P. Leone, A comparative assessment on hydrogen production from low- and high-temperature electrolysis, Int. J. Hydrogen Energy 38 (2013) 3523–3536, https://doi.org/10.1016/j.ijhydene.2013.01.065.

[3] R. Küngas, Review—electrochemical CO_2 reduction for CO production: comparison of low- and high-temperature electrolysis technologies, J. Electrochem. Soc. 167 (2020), 044508, https://doi.org/10.1149/1945-7111/ab7099.

[4] C. Graves, S.D. Ebbesen, M.B. Mogensen, K.S. Lackner, Sustainable hydrocarbon fuels by recycling CO_2 and H_2O with renewable or nuclear energy, Renew. Sustain. Energy Rev. 15 (2011) 1–23, https://doi.org/10.1016/j.rser.2010.07.014.

[5] M.B. Mogensen, M. Chen, H.L. Frandsen, C. Graves, J.B. Hansen, K.V. Hansen, A. Hauch, T. Jacobsen, S.H. Jensen, T.L. Skafte, X. Sun, Reversible Solid-Oxide Cells for Clean and Sustainable Energy, Clean Energy, 2019, pp. 1–27, https://doi.org/10.1093/ce/zkz023.

[6] V. Venkataraman, M. Pérez-Fortes, L. Wang, Y.S. Hajimolana, C. Boigues-Muñoz, A. Agostini, S.J. McPhail, F. Maréchal, J. van Herle, P.V. Aravind, Reversible solid oxide systems for energy and chemical applications – review & perspectives, J. Energy Storage 24 (2019) 100782, https://doi.org/10.1016/j.est.2019.100782.

[7] S.H. Jensen, C. Graves, M.B. Mogensen, C. Wendel, R. Braun, G. Hughes, Z. Gao, S. A. Barnett, Large-scale electricity storage utilizing reversible solid oxide cells combined with underground storage of CO_2 and CH_4, Energy Environ. Sci. 8 (2015) 2471–2479, https://doi.org/10.1039/C5EE01485A.

[8] A. Hauch, R. Küngas, P. Blennow, A.B. Hansen, J.B. Hansen, B.V. Mathiesen, M. B. Mogensen, Recent advances in solid oxide fuel cell technology, Science 370 (2020), https://doi.org/10.1126/science.aba6118.

[9] Final Report for Energinet.dk project no. 2013-1-12013 M. Chen, A. Hauch, K. Brodersen, B. Charlas, Solid Oxide Electrolysis for Grid Balancing Index, 2015, https://doi.org/10.13140/RG.2.2.20291.09760.

[10] M. Lang, S. Raab, M.S. Lemcke, C. Bohn, M. Pysik, Long-term behavior of a solid oxide electrolyzer (SOEC) stack, Fuel Cell. 20 (2020) 690–700, https://doi.org/10.1002/fuce.201900245.

[11] Y. Wang, A. Banerjee, O. Deutschmann, Dynamic behavior and control strategy study of CO_2/H_2O co-electrolysis in solid oxide electrolysis cells, J. Power Sources 412 (2019) 255–264, https://doi.org/10.1016/j.jpowsour.2018.11.047.

[12] L. Zhang, X. Li, J. Jiang, S. Li, J. Yang, J. Li, Dynamic modeling and analysis of a 5-kW solid oxide fuel cell system from the perspectives of cooperative control of thermal safety and high efficiency, Int. J. Hydrogen Energy 40 (2015) 456–476, https://doi.org/10.1016/j.ijhydene.2014.10.149.

[13] T.L. Skafte, Z. Guan, M.L. Machala, C.B. Gopal, M. Monti, L. Martinez, E. Stamate, S. Sanna, J.A. Garrido Torres, E.J. Crumlin, M. García-Melchor, M. Bajdich, W. C. Chueh, C. Graves, Selective high-temperature CO_2 electrolysis enabled by oxidized carbon intermediates, Nat. Energy 4 (2019) 846–855, https://doi.org/10.1038/s41560-019-0457-4.

[14] A. Hauch, M.L. Traulsen, R. Küngas, T.L. Skafte, CO_2 electrolysis – gas impurities and electrode overpotential causing detrimental carbon deposition, J. Power Sources 506 (2021) 230108, https://doi.org/10.1016/j.jpowsour.2021.230108.

[15] J. Suk Kim, M. McKellar, S.M. Bragg-Sitton, R.D. Boardman, Status on the Component Models Developed in the Modelica Framework: High-Temperature Steam Electrolysis Plant & Gas Turbine Power Plant, United States), Idaho Falls, ID, 2016, https://doi.org/10.2172/1333156.

[16] M.B. Mogensen, Thermodynamics of High Temperature H_2O and CO_2 Electrolysis, Figshare, 2020, https://doi.org/10.6084/m9.figshare.12652322.

[17] J. Schefold, A. Brisse, A. Surrey, C. Walter, 80,000 current on/off cycles in a one year long steam electrolysis test with a solid oxide cell, Int. J. Hydrogen Energy 45 (2020) 5143–5154, https://doi.org/10.1016/j.ijhydene.2019.05.124.

[18] M. Chen, Y.-L. Liu, J.J. Bentzen, W. Zhang, X. Sun, A. Hauch, Y. Tao, J.R. Bowen, P. V. Hendriksen, Microstructural degradation of Ni/YSZ electrodes in solid oxide electrolysis cells under high current, J. Electrochem. Soc. 160 (2013) F883–F891, https://doi.org/10.1149/2.098308jes.

[19] Y. Tao, S.D. Ebbesen, M.B. Mogensen, Degradation of solid oxide cells during co-electrolysis of steam and carbon dioxide at high current densities, J. Power Sources 328 (2016) 452–462, https://doi.org/10.1016/j.jpowsour.2016.08.055.

[20] A. Hauch, K. Brodersen, M. Chen, M.B. Mogensen, Ni/YSZ electrodes structures optimized for increased electrolysis performance and durability, Solid State Ionics 293 (2016) 27–36, https://doi.org/10.1016/j.ssi.2016.06.003.

[21] C. Graves, S.D. Ebbesen, S.H. Jensen, S.B. Simonsen, M.B. Mogensen, Eliminating degradation in solid oxide electrochemical cells by reversible operation, Nat. Mater. 14 (2015) 239–244, https://doi.org/10.1038/nmat4165.

[22] Q. Fu, J. Schefold, A. Brisse, J.U. Nielsen, Durability testing of a high-temperature steam electrolyzer stack at 700 °C, Fuel Cell. 14 (2014) 395–402, https://doi.org/10.1002/fuce.201300150.

[23] S.D. Ebbesen, C. Graves, A. Hauch, S.H. Jensen, M.B. Mogensen, Poisoning of solid oxide electrolysis cells by impurities, J. Electrochem. Soc. 157 (2010) B1419–B1429, https://doi.org/10.1149/1.3464804.

[24] N. Bonanos, B.C.H. Steele, E.P. Butler, Applications of impedance spectroscopy, in: E. Barsoukov, J.R. Macdonald (Eds.), Impedance Spectroscopy: Theory, Experiment, and Applications, John Wiley & Sons, Inc., Hoboken, NJ, USA, 2018, p. 230, https://doi.org/10.1002/9781119381860.

[25] C. Graves, RAVDAV Data Analysis Software, 2015, version 0.9.8.

[26] Y. Zheng, Q. Li, W. Guan, C. Xu, W. Wu, W.G. Wang, Investigation of 30-cell solid oxide electrolyzer stack modules for hydrogen production, Ceram. Int. 40 (2014) 5801–5809, https://doi.org/10.1016/j.ceramint.2013.11.020.

[27] W. Guan, W.G. Wang, Electrochemical performance of planar solid oxide fuel cell (SOFC) stacks: from repeat unit to module, Energy Technol. 2 (2014) 692–697, https://doi.org/10.1002/ente.201402015.

[28] K. Thydén, Y.L. Liu, J.B. Bilde-Sørensen, Microstructural characterization of SOFC Ni-YSZ anode composites by low-voltage scanning electron microscopy, Solid State Ionics 178 (2008) 1984–1989, https://doi.org/10.1016/j.ssi.2007.12.075.

[29] M. Navasa, X.-Y. Miao, H.L. Frandsen, A fully-homogenized multiphysics model for a reversible solid oxide cell stack, Int. J. Hydrogen Energy 44 (2019) 23330–23347, https://doi.org/10.1016/j.ijhydene.2019.06.077.

[30] X.-Y. Miao, O.B. Rizvandi, M. Navasa, H.L. Frandsen, Modelling of local mechanical failures in solid oxide cell stacks, Appl. Energy 293 (2021) 116901, https://doi.org/10.1016/j.apenergy.2021.116901.

[31] O. Babaie Rizvandi, X.-Y. Miao, H.L. Frandsen, Multiscale modeling of degradation of full solid oxide fuel cell stacks, Int. J. Hydrogen Energy (2021), https://doi.org/10.1016/j.ijhydene.2021.05.204.

[32] M. Navasa, C. Graves, C. Chatzichristodoulou, T.L. Skafte, B. Sundén, H. L. Frandsen, A three dimensional multiphysics model of a solid oxide electrochemical cell: a tool for understanding degradation, Int. J. Hydrogen Energy 43 (2018) 11913–11931, https://doi.org/10.1016/j.ijhydene.2018.04.164.

[33] T.L. Skafte, P. Blennow, J. Hjelm, C. Graves, Carbon deposition and sulfur poisoning during CO_2 electrolysis in nickel-based solid oxide cell electrodes, J. Power Sources 373 (2018) 54–60, https://doi.org/10.1016/j.jpowsour.2017.10.097.

[34] M. Navasa, H.L. Frandsen, T.L. Skafte, B. Sundén, C. Graves, Localized carbon deposition in solid oxide electrolysis cells studied by multiphysics modeling, J. Power Sources 394 (2018) 102–113, https://doi.org/10.1016/j.jpowsour.2018.05.039.

[35] F. Tietz, D. Sebold, A. Brisse, J. Schefold, Degradation phenomena in a solid oxide electrolysis cell after 9000 h of operation, J. Power Sources 223 (2013) 129–135. http://linkinghub.elsevier.com/retrieve/pii/S0378775312014826. (Accessed 29 July 2014).

[36] X. Sun, P.V. Hendriksen, M.B. Mogensen, M. Chen, Degradation in solid oxide electrolysis cells during long term testing, Fuel Cell. 19 (2019) 740–747, https://doi.org/10.1002/fuce.201900081.

[37] X. Sun, B.R. Sudireddy, X. Tong, M. Chen, K. Brodersen, A. Hauch, Optimization and durability of reversible solid oxide cells, ECS Transactions 91 (2019) 2631–2639, https://doi.org/10.1149/09101.2631ecst.

[38] M. Trini, A. Hauch, S. de Angelis, X. Tong, P.V. Hendriksen, M. Chen, Comparison of microstructural evolution of fuel electrodes in solid oxide fuel cells and electrolysis cells, J. Power Sources 450 (2020) 227599, https://doi.org/10.1016/j.jpowsour.2019.227599.

[39] A. Hauch, S.H. Jensen, J.B. Bilde-Sørensen, M.B. Mogensen, Silica segregation in the Ni/YSZ electrode, J. Electrochem. Soc. 154 (2007) A619, https://doi.org/10.1149/1.2733861.

[40] W. Choi, P.N. Enjeti, A.J. Appleby, An advanced power converter topology to significantly improve the CO tolerance of the PEM fuel cell power systems, in: Conference Record of the 2004 IEEE Industry Applications Conference, 2004. 39th IAS Annual Meeting, IEEE, 2004, pp. 1185–1191, https://doi.org/10.1109/IAS.2004.1348563.

[41] P.J. Sarma, C.L. Gardner, S. Chugh, A. Sharma, E. Kjeang, Strategic implementation of pulsed oxidation for mitigation of CO poisoning in polymer electrolyte fuel cells, J. Power Sources 468 (2020) 228352, https://doi.org/10.1016/j.jpowsour.2020.228352.

[42] S.H. Jensen, A. Hauch, X. Sun, M. Chen, S.D. Ebbesen, M.B. Mogensen, Diffusion rates of reactants and components in solid oxide cells, Proceedings of the 13th European SOFC & SOE Forum B1208 (2018) 71–82, 2018.

[43] R. Kungas, P. Blennow, T. Heiredal-Clausen, T. Holt Nørby, D. Rasmussen, J. Rass-Hansen, P.G. Moses, J. Hansen, Commercialization of CO_2 electrolysis by haldor Topsoe, ECS Meeting Abstracts (2021), https://doi.org/10.1149/MA2021-031191mtgabs. MA2021-03.

[44] Q. Fang, C.E. Frey, N.H. Menzler, L. Blum, Electrochemical performance and preliminary post-mortem analysis of a solid oxide cell stack with 20,000 h of operation, J. Electrochem. Soc. 165 (2018) F38–F45, https://doi.org/10.1149/2.0541802jes.

[45] M.B. Mogensen, M. Chen, H.L. Frandsen, C. Graves, A. Hauch, P.V. Hendriksen, T. Jacobsen, S.H. Jensen, T.L. Skafte, X. Sun, Ni migration in solid oxide cell electrodes: review and revised hypothesis, Fuel Cell. (2021), https://doi.org/10.1002/fuce.202100072 fuce.202100072.

[46] K. Thyden, Microstructural characterization of SOFC Ni–YSZ anode composites by low-voltage scanning electron microscopy, Solid State Ionics 178 (2008) 1984–1989, https://doi.org/10.1016/j.ssi.2007.12.075.